Thermal Chemistry of CH_3 on Si/Cu(100); the Role of Sn as a Promoter

Xiang V. Zhang and Daniel R. Strongin*

Department of Chemistry, Temple University, Philadelphia, Pennsylvania 19122

L. V. Goncharova, A. V. Ermakov, and B. J. Hinch

Department of Chemistry and Chemical Biology, Wright-Rieman Laboratories, Laboratory for Surface Modification, Rutgers University, 610 Taylor Rd, Piscataway, New Jersey 08854

Received: June 28, 2004

The effect of tin on the thermal chemistry of CH_3 on Si/Cu(100) was investigated using temperature programmed desorption (TPD), X-ray photoelectron spectroscopy (XPS), ion scattering spectroscopy (ISS), low energy electron diffraction (LEED), Auger electron spectroscopy (AES), and high-resolution helium atom scattering (HAS). The Si/Cu(100) substrate was prepared by exposure to silane at 420 K. The TPD results showed that $(CH_3)_3SiH$ was the dominant product desorbing from Si/Cu(100) after exposure to CH_3 radical, and that its desorption was sensitive to the concentration of Si in the outermost surface. For the silane-saturated surface, Si^{sat}/Cu(100), $(CH_3)_3SiH$ desorbed near 500 K, while for subsaturated surfaces, Si^{unsat}/Cu(100), $(CH_3)_3SiH$ desorbed at both 270 and 500 K. The addition of Sn to the Si^{sat}/Cu(100) surface, prior to CH_3 exposure, led to a shift in the $(CH_3)_3SiH$ desorption feature to higher temperatures. Tin addition to Si^{unsat}/Cu(100) surface changed the product distribution. Specifically, with Sn coadsorption levels in excess of 0.7 ML, the dominant product is the fully methylated species, $(CH_3)_4Si$, at 430 K.

1. Introduction

The Rochow, or Direct, Synthesis, which involves the reactions of CH_3Cl on Si/Cu based surfaces, is used in industry to produce methylchlorosilanes, which are precursors for production of silicone materials.[1] Due to the importance of the silicone applications, the Direct Synthesis has been studied intensively for more than half a century.[2−9] The large majority of the studies was performed under reaction conditions that are similar to those in the production line (using fluidized bed reactors or stirred bed reactors), and they evaluated the effects of reaction parameters on the methylchlorosilane yield and selectivity. The mechanism for methylchlorosilane production, however, is still not understood on a molecular scale, in part because of the complexity of the multicomponent catalyst. The Direct Synthesis catalyst is predominately composed of Si/Cu, but the material also contains promoter elements (e.g., Sn, Zn, and Al) that are essential for the commercially viable operation of the industrial catalyst. A substantial fraction of research in this area has focused on empirical observations of the promoter-induced effects on yield and selectivity of the Direct Synthesis reaction. This approach produced an efficient industrial catalyst, but has not yielded a detailed molecular-level understanding of the promoters. We argue that this level of understanding is required for modifications in the catalyst operation for future applications.

Both the yield and selectivity of methylchlorosilane production are affected significantly by the presence of Sn in the industrial Si/Cu catalyst. Despite controversies, and often contradictory results,[5,10−12] arising from different impurity levels in reactant feeds, most researchers have agreed that tin can promote the Direct Synthesis synergistically with zinc or aluminum. One proposed activating mechanism is that tin facilitates methylization of surface silicon by transporting methyl groups as tin/methyl complexes on the reacting surface.[10] The transfer of methyl from tin to silicon atoms is not unexpected energetically, as the Si−CH_3 bond strength is greater than that of a Sn−CH_3 bond.[13]

A less extensive body of research, using surface science techniques in vacuum environments on polycrystalline and single crystal Si/Cu surfaces (without promoter atoms), has also concentrated on the Direct Synthesis. Initially, the interactions of CH_3 and/or Cl monolayers on Si/Cu surfaces were studied.[14−18] The present contribution builds on these prior studies and makes the first UHV controlled investigations of the effects of Sn on the thermal chemistry of CH_3 on Si/Cu(100). In this study, we use a combination of TPD, XPS, ISS, LEED, AES, and HAS to investigate the formation of Sn/Si/Cu(100) structures and to elucidate new methylsilane desorption mechanisms in the presence of surface bound Sn. Our results concerning the effect of Sn on the thermal chemistry of CH_3 on Si/Cu(100) start to develop a microscopic surface picture of how Sn facilitates the Direct Synthesis.

2. Experimental Section

Two ultrahigh vacuum experimental systems were used to obtain the results presented in this contribution. TPD, XPS, and ISS data were acquired in the first system, and LEED, AES, and high-resolution HAS studies were conducted in a second system. Both UHV chambers had base pressures below 2×10^{-10} Torr.

To carry out TPD experiments, the Cu single crystal sample was mounted on a tantalum plate, and this assembly was in good thermal contact with a liquid nitrogen cryostat. In this arrangement, the sample could be cooled to 100 K, and using

* To whom correspondence should be addressed. Tel#(215)204-7119. Fax#(215)204-1532, E-mail: dstrongi@temple.edu.

10.1021/jp0471960 CCC: $27.50 © 2004 American Chemical Society
Published on Web 09/17/2004

resistive heating the sample temperature could be raised to 900 K, as measured with a thermocouple (K type). All TPD experiments presented in this contribution used a heating rate of 3 K/s. Gas species desorbing from the surface were analyzed with a quadrupole mass spectrometer (UTI). Reference cracking patterns of the pure di-, tri-, and tetramethylsilanes were used for the identification of desorbing species during TPD.

XPS data were acquired with unmonochromatized Mg Kα (1253.6 eV) radiation. The pass energy of the 100 mm hemispherical analyzer was set at 50 eV during the acquisition of core-level data. The binding energy scale for the XPS was calibrated against pure reference metals. The ISS was carried out by using a 1000 eV incident He^+ beam at 45° from the surface normal. The pass energy of the hemispherical analyzer was fixed at 75 eV for these experiments.

In the second system, the sample could be cooled to liquid nitrogen temperatures or heated to 900 K by electron beam bombardment. Intermediate temperatures were controlled by radiative heating from the neighboring W filament alone. The sample temperature was also monitored with type K thermocouples. Both helium atom and electron diffraction data were taken in this chamber; this system has been described in detail elsewhere.[19] Auger measurements were taken with a PHI double pass cylindrical mirror analyzer.

In both systems, Cu(100) crystals were cleaned by 30 min cycles of 1500 eV Ar^+ sputtering followed by 850 K annealing. The higher sputtering voltage (1500 V) was often needed to remove the residual surface tin atoms. After sputter cleaning, no surface tin, oxygen, or carbon contaminants were observed, either by XPS or by Auger spectroscopy.

The Si/Cu(100) surfaces were prepared by exposing Cu(100) surfaces to 5% SiH_4/Ar mixtures. The Cu samples were kept at 420 K during the silicon deposition to desorb surface hydrogen. Two distinct Si/Cu surface preparations were used in the studies (in both systems) and will be carefully distinguished, as different desorption behavior was observed from the two Si/Cu(100) surfaces. (i) The Si-saturated surface, which will be referred to as the Si^{sat}/Cu(100), was prepared by exposing the Cu samples to more than 6 L of SiH_4 (i.e., 1×10^{-6} Torr × 120 s × 5%). Previous studies of the Si-saturated Cu(100) surface have shown that the Si coverage reaches 0.4 ML and the top layer has a Cu_2Si stoichiometry.[20] (ii) For the subsaturation silicon density films, SiH_4 exposures of 5 L were used; the latter produces a silicon coverage of 0.13 ML only. This second type of (Si unsaturated) surface is referred to as the Si^{unsat}/Cu(100) surface.

Comparable Sn evaporation sources were used in both experimental systems. In the first system, Sn was deposited onto the Cu and Si/Cu surfaces at approximately 200 K. The surface tin coverage was calibrated relative to the saturated surface Si coverage of 0.4 ML, using XPS and published cross sections for Sn 3d and Si 2p core levels using Mg Kα radiation as the excitation source. In the second system, both silane adsorption and tin deposition were first monitored in helium atom specular reflectivity measurements, in a range of substrate temperatures. (The specular condition uses equal incident and emerging angles, $\Theta_i = \Theta_f = 49.5°$.) The Sn deposition was monitored with a quartz microbalance. Auger spectra were also recorded after each deposition, and ratios, between the Sn(MNN) peak at 430 eV and the Cu(LMM) peak at 920 eV, were used for calibration purposes.

The CH_3 radicals were generated by the thermal pyrolysis of azomethane.[21] Prior studies have shown that the Si/Cu surface was saturated with CH_3 after a "5 L" exposure to azomethane.[14] In this study, a "12 L" exposure was used to guarantee surface saturation of methyl species at 173 K. Note that here the nominal azomethane exposure is measured with a remote uncalibrated ionization gauge measuring a total gas pressure, comprising the desired CH_3 radical, a byproduct N_2, and the parent molecule CH_3NNCH_3, as well as low concentrations of other possible byproducts. The quoted exposures, therefore, can only be relative.

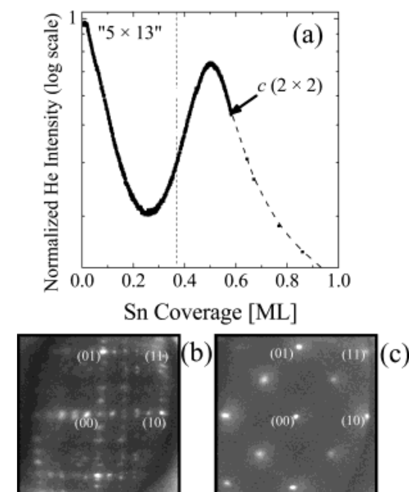

Figure 1. (a) Variation of specular helium reflectivity during Sn deposition on the Si^{sat}/Cu(100) surface ($T_x = 173$ K, $E_i = 21.7$ meV). LEED patterns measured prior to Sn deposition indicating a (5 × 13) reconstruction of the Si^{sat}/Cu(100) surface (b), and the c(2 × 2) pattern measured after deposition of 0.6 ML Sn on the original Cu_2Si Cu(100) film (c). Incident electron energies of 90−100 eV were used. The dashed vertical line in (a) indicates the onset of structures with the c(2 × 2) diffraction intensities.

3. Results

3.1. Structural Studies of Sn/Si/Cu(100). 3.1.1. Helium Reflectivity and LEED Studies of Sn on Si^{sat}/Cu(100). Figure 1a shows the specularly reflected helium intensity from a Si^{sat}/Cu(100) surface during the deposition of Sn at 173 K. The fast decline with respect to that of the Sn-free surface is indicative of Sn sticking and increased disorder and roughness at the surface. The intensity recovery indicates the onset of reordering and the optimization of a superstructure at 0.5 ML of Sn. Further Sn deposition results in a second specular intensity drop; we presume that the latter drop is associated with the start of multilayer film growth. Multiple oscillations in the He intensity have not been observed at this surface growth temperature. The continuous curve of Figure 1a represents the He intensity during one deposition period, and the data points represent the measured intensities after subsequent growth periods. (Interruptions were necessary only for monitoring of helium and LEED diffraction intensities.) Figures 1b and c exhibit LEED patterns for the Si^{sat}/Cu(100) structure, before and after 0.60 ML of Sn was deposited, at 173 K. The surface structure of Si^{sat}/Cu(100) is associated with a (5 × 13) diffraction pattern; this is consistent with prior studies.[20] Also, the exposure of this surface, at 173 K, to 0.60 ML Sn led to a c(2 × 2) structure. This experimental observation suggests that the unusual hexagonal-like surface symmetry, associated with the outermost surface layer of Si^{sat}/Cu(100), is restored to the substrate's square symmetry with the addition of Sn. Additional experiments showed that the c(2 × 2) pattern was attained, and islanding occurs, even at Sn coverages as low as 0.35 ML.

Heating of the 0.6 ML Sn/Si^{sat}/Cu(100) surface to temperatures above 375 K led to the evolution of the p($\sqrt{2}$ × 3

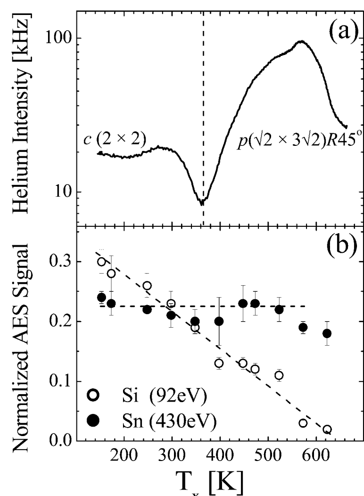

Figure 2. Variation of the helium specular reflectivity (a) and normalized AES signals of Si and Sn (b) during thermal ramping of a 0.6 ML Sn/Si^{sat}/Cu(100) surface. The ramp rate is of the order of 2 K/s for curve (a). The data shown in (b) are taken after successive anneals, each for 120 s, and cooling to ~150 K. Note also that the helium intensity is plotted on a logarithmic scale.

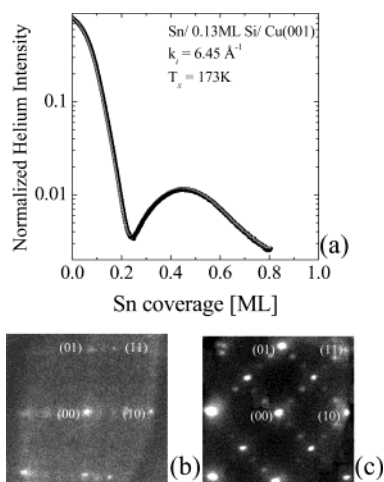

Figure 3. (a) He reflectivity during Sn deposition (uptake curve) on a subsaturated Si^{unsat}/Cu(100) surface ($\Theta_i = 49.5°$, $E_i = 21.7$ meV) and LEED patterns of the Cu(100) surface with small fractional area covered with (5 × 13) reconstructed Cu_2Si patches (b), and with the p($\sqrt{2}$ × 3$\sqrt{2}$)R45° superstructure after deposition of 0.6 ML Sn (c). An incident electron energy of 100 eV was used and the surface temperature of all measurements was 173 K.

$\sqrt{2}$)R45° phase. This transition is emphasized by helium reflectivity data shown in Figure 2a that plot the helium intensity versus surface temperature for 0.6 ML Sn/Si^{sat}/Cu(100). These data show that, as the surface temperature is raised above 400 K, there is an increased ordering of the surface layer. Figure 2b exhibits Si and Sn AES data that indicate that while the concentration of Sn is stable throughout the 173−500 K range, the concentration of Si shows a monotonic decrease. Some Si does persist at 500 K, but, at 600 K, Si is essentially absent from the Auger spectra of the near surface region.

3.1.2. Helium Reflectivity, LEED, and ISS Studies of Sn on Si^{unsat}/Cu(100). Figure 3a exhibits the variation of helium reflectivity data for a Si^{unsat}/Cu(100) surface as a function of Sn coverage. The Sn-free surface exhibits a rather diffuse (5 × 13) LEED pattern (Figure 3b). The diffuse 5 × 13 pattern is consistent with prior scanning tunneling microscopy and helium diffraction data that show that, at these relatively low Si coverages, the 5 × 13 domains can coexist with disordered

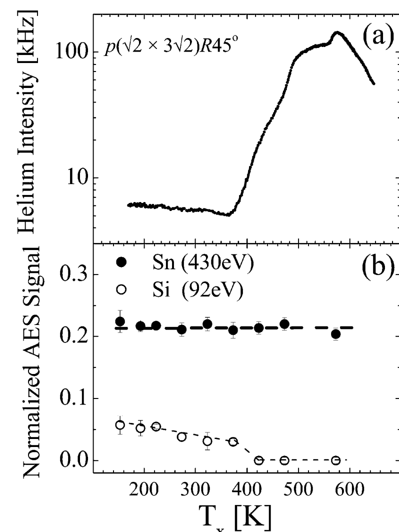

Figure 4. Variation of the specular helium intensity (a) and normalized AES signals of Si and Sn (b), as a function of surface temperature for the subsaturation silicon coverage surface following deposition of 0.65 ML Sn.

domains that have higher Cu to Si stoichiometric ratios. As Sn is continuously added to the surface at 173 K, to a coverage of 0.2 ML, there is a drop in the helium reflectivity intensity and in the quality of the (5 × 13) LEED pattern (not shown). This is indicative of a decrease in surface ordering. There is a rapid increase in the helium reflectivity intensity above a Sn coverage of 0.3 ML, and LEED also shows the evolution of a p($\sqrt{2}$ × 3 $\sqrt{2}$)R45° LEED pattern. Figure 3c exhibits a sharp p($\sqrt{2}$ × 3 $\sqrt{2}$)R45° LEED pattern that was obtained at a Sn coverage of 0.6 ML. At still higher Sn coverages there is a continuous degradation of surface order, and at a Sn coverage of 0.8 ML (not shown) long range order is not observed in either helium or electron diffraction.

Figure 4a exhibits helium reflectivity data for a 0.65 ML Sn/ Si^{unsat}/Cu(100) surface, which exhibits a poor p($\sqrt{2}$ × 3 $\sqrt{2}$)R45° LEED pattern at 173 K and much better ordering after heating to 600 K. The reflectivity data show a rapid intensity increase near 400 K that is sustained to a temperature of 600 K. The symmetry of the p($\sqrt{2}$ × 3$\sqrt{2}$)R45° LEED pattern is maintained throughout this increase in helium reflectivity intensity. Figure 4b exhibits Si and Sn AES data and indicates that the Sn concentration is stable throughout the annealing to 600 K. There, however, is a marked decrease in the concentration of Si in the near surface region as the surface is annealed to 400 K. By 410 K, there is no evidence of Si in the near surface region in the Auger data.

Figure 5 exhibits ISS data for Cu(100) and Si^{unsat}/Cu(100), after 0.37 ML of Sn is deposited on Si^{unsat}/Cu(100), and after this Sn/Si^{unsat}/Cu(100) surface is heated to 420 K momentarily and then cooled back to 150 K. After deposition of Sn at 200 K, there is a marked decrease in both the Si and Cu ISS features. Annealing the surface to 420 K results in an increase in the Cu peak intensity (by more than a factor of 2) to a level similar to that of the Si^{unsat}/Cu(100) surface. The Si ISS feature intensity for Sn/Si^{unsat}/Cu(100) after annealing to 420 K (Figure 5d) is also increased, although it is still approximately 50% of that associated with the same feature in the Si^{unsat}/Cu(100) data (Figure 5b). This result suggests that while Si can emerge from under Sn to the outermost surface (during annealing), at least some Si leaves the outermost surface during Sn deposition or after the annealing process. This experimental observation is

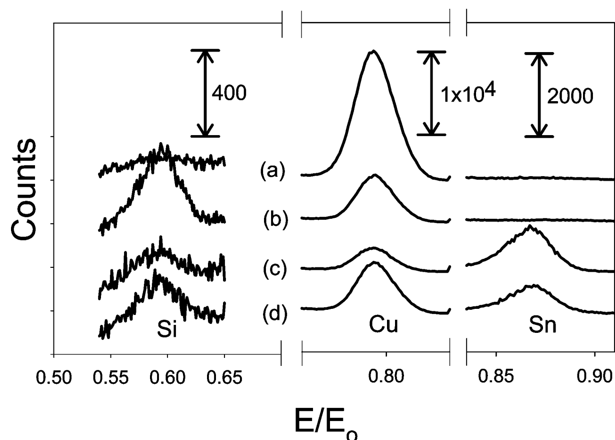

Figure 5. Successive He^+ ISS scans, each taken at 150 K, during production of a 0.37 ML Sn/Si^{unsat}/Cu(100) surface. (a) Cu(100); (b) Si^{unsat}/Cu; (c) Sn/Si/Cu; (d) after the sample was annealed to 420 K and returned to 150 K, where the spectra was obtained. An $E_0 = 1000$ eV was used to obtain these data.

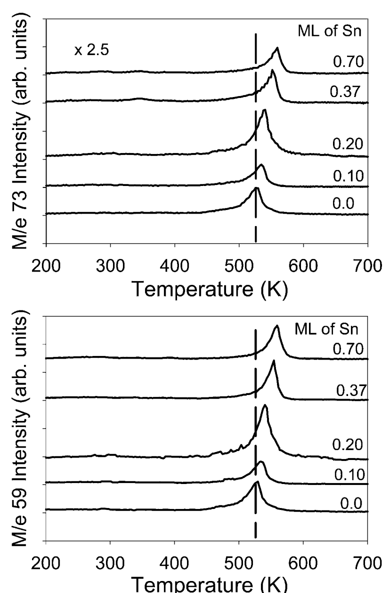

Figure 6. TPD from CH_3^{sat}/Sn/Si^{sat}/Cu(100) as a function of surface Sn coverage. The initial (saturated) silicon concentration was identical for each run (0.4 ML). The *m*/*e* value of 59 is associated with the $(CH_3)_2$-SiH^+ ion intensity and *m*/*e* 73 shows the $(CH_3)_3Si^+$ ion intensity.

consistent with the AES data (Figure 4b) that show a continuous decrease in Si concentration as the Sn/Si^{unsat}/Cu(100) surface is heated above the 173 K deposition temperature. Arguably, the AES data are, and should be, a little less sensitive to any degree of Si emergence (from under Sn), as the Auger spectroscopy intrinsically has a slightly larger sensitivity depth than the ISS data.

3.2. Temperature Programmed Desorption Studies. 3.2.1. Sn Deposition on the Si^{sat}/Cu(100) Surface. Figure 6 exhibits TPD data for CH_3^{sat}/Sn/Si^{sat}/Cu(100). Various coverages of Sn were deposited on Si^{sat}/Cu(100) substrates, after which the three-component surfaces (Sn/Si^{sat}/Cu) were saturated with CH_3 radicals. The TPD data show that $(CH_3)_3SiH$ [3MS], experimentally observed at *m*/*e* values of both 59 and 73, has a temperature desorption maximum at 520 K, and it is the dominant product desorbing from the Sn-free Si^{sat}/Cu(100). This $(CH_3)_3SiH$ species remains the dominant desorption product with the coadsorption of Sn, although the T_{max3MS} associated with this product increases with the Sn coverage. At the highest Sn coverage used, T_{max3MS} shifted to 560 K, a 40 K increase relative to that of the Sn-free surface.

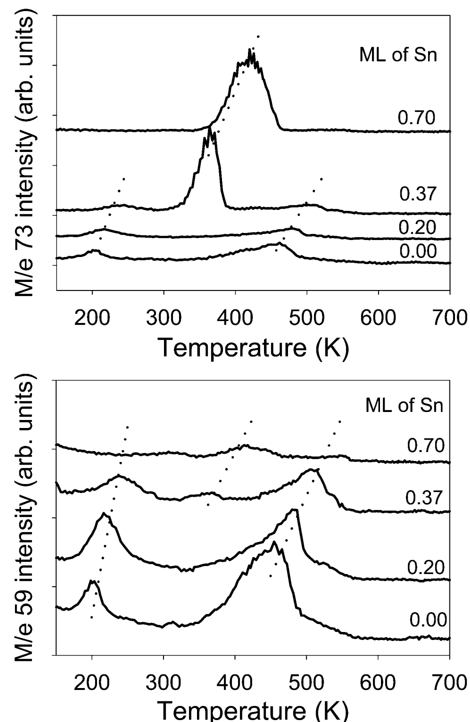

Figure 7. The *m*/*e* values of 59 and 73 TPD from CH_3^{sat}/Sn/Si^{unsat}/Cu(100) as a function of surface Sn coverage. The *m*/*e* value of 59 shows the $(CH_3)_2SiH^+$ ion intensity and *m*/*e* 73 shows the $(CH_3)_3Si^+$ ion intensity.

3.2.2. Sn Deposition on Submonolayer Si/Cu(100). Figure 7 displays a TPD series for the Si^{unsat}/Cu(100) surface, each with an initial Si coverage of 0.13 ML. Consistent with earlier data,[14] TPD data for the Sn-free surface, with a saturation coverage of CH_3, showed two desorption peaks with temperature maxima of 220 and 470 K. The predominant product associated with both desorption states was $(CH_3)_3SiH$. Significant changes in the TPD profile, however, occurred when coadsorbed Sn was present. Perhaps most notably, as the coverage of Sn increased, the yield of $(CH_3)_3SiH$ (monitored at *m*/*e* 59) decreased and there was a concomitant increase in the yield of tetramethylsilane, $(CH_3)_4Si$ [4MS]. This desorbing product yielded a strong signal at a *m*/*e* value of 73 and, as expected, it was not detected in the *m*/*e* 59 spectrum. At a Sn coverage of 0.37 ML, T_{max4MS} for $(CH_3)_4Si$ was 375 K and at the highest Sn coverage investigated (0.7 ML), T_{max4MS} shifted to 420 K. The fully methylated $(CH_3)_4Si$ product accounted for ~85% of the desorbing product at the highest Sn coverage. Also, while Sn decreased the yield of $(CH_3)_3SiH$, there were associated shifts of the two T_{max3MS} for this product to higher temperatures.

3.2.3. TPD of $(CH_3)_4Sn$ Adsorbed on Si/Cu(100). Complimentary TPD results were obtained for the Si/Cu(100) surface after the adsorption of tetramethyl tin, $(CH_3)_4Sn$. Figure 8 exhibits individual TPD spectra that were obtained after the unsaturated and saturated Si/Cu(100) surfaces were exposed to 10 L of $(CH_3)_4Sn$. The TPD data for both surfaces are qualitatively the same. Specifically, the predominate product desorbing from both surfaces is $(CH_3)_3SiH$ and this product is associated with T_{max3MS} values of 230 and 460 K. The intensity of the 460 K peak for the 0.13 ML Si/Cu(100) surface was, however, consistently greater than the analogous peak associated with the saturated Si/Cu(100) surface.

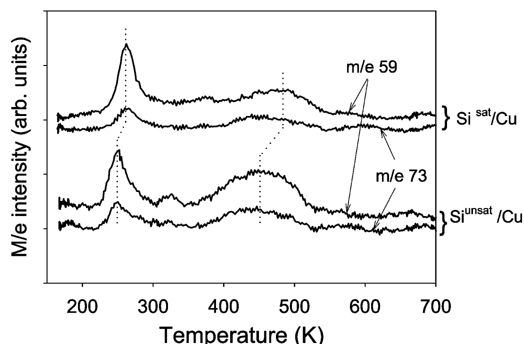

Figure 8. TPD from $Sn(CH_3)_4$/Si/Cu(100) for the Si-saturated Cu surface Si^{sat}/Cu(100), and the Si-unsaturated Cu surface, Si^{unsat}/Cu(100). The *m*/*e* value of 59 shows the $(CH_3)_2SiH^+$ ion intensity and *m*/*e* 73 shows the $(CH_3)_3Si^+$ ion intensity.

4. Discussion

Results for this study, as well as earlier research, have shown that the dominant desorption product during CH_3-TPD, either from Si^{sat}/Cu(100) or from Sn-free Si^{unsat}/Cu(100), is $(CH_3)_3$-SiH. The TPD data presented in Figures 6−8 show that $(CH_3)_3$-SiH desorbs in two states with T_{max3MS} of roughly 300 and 500 K, while only one $(CH_3)_3$SiH desorption state, at ∼500 K, is associated with Si^{sat}/Cu(100). Our earlier STM research has suggested that the Si^{unsat}/Cu(100) surface is not uniform.[22] The surface contains patches of ordered 5 × 13 [Cu_2Si, i.e., Si^{sat}/Cu(100)] coexisting with disordered patches with much lower Si concentrations. The 500 K desorption state was attributed to the reactions of CH_3 on 5 × 13 domains, and the 300 K desorption state to the disordered domains, with lower Si concentrations.[14] The Si^{sat}/Cu(100) surface consists entirely of 5 × 13 domains and, hence, only exhibits the high temperature $(CH_3)_3$SiH desorption state during CH_3 TPD.

Studies using coadsorbed hydrogen, on the Sn-free surfaces, have indicated that at 500 K the rate-limiting step for $(CH_3)_3$-SiH desorption, from Si^{sat}/Cu regions, is that of methyl cracking.[14] The completion of the two $(CH_3)_3$SiH desorption peaks associated with CH_3/Si^{unsat}/Cu(100) are thus believed to be associated with the reaction and depletion of all CH_3, through subsequent desorption of $(CH_3)_3$SiH, from each of the two distinct patches that characterize this surface. This explanation requires that CH_3 is *not* (highly) mobile on the Si rich regions, since *if* this were the case all the CH_3 would be expected to migrate and crack or desorb as $(CH_3)_3$SiH on Cu rich regions below 500 K (i.e., the 500 K peak would not be present).

With this aspect of the $(CH_3)_3$SiH desorption mechanism in mind, together with the assumption that the adsorbed methyl species does not strongly influence the Sn/Si/Cu surface structure, we shall discuss our present data. The most significant observation is that the addition of Sn to the Si^{unsat}/Cu(100) surface (at Sn coverages higher than 0.3 ML) results in a new desorption channel (at intermediate temperatures) with the formation of a new product, $(CH_3)_4$Si.

4.1. Sn Deposition on the Si-Saturated Cu(100) Surface. There is a significant structural change of the Si^{sat}/Cu(100) surface with the addition of Sn. Specifically, starting at a Sn coverage of 0.35 ML, there is a transition from the 5 × 13, associated with clean Si^{sat}/Cu(100), into a c(2 × 2) ternary Sn/Si/Cu(100) phase. The CH_3-TPD results suggest that this structural change does not have an experimentally observable effect on the product distribution. The T_{max3MS}, associated with $(CH_3)_3$SiH desorption, only shows a shift to higher temperatures with increasing Sn coverage. At the highest Sn coverage investigated (0.7 ML), T_{max3MS} has increased by ∼40 K. As the rate-limiting step for $(CH_3)_3$SiH desorption on the Si-saturated surface is C−H bond cleavage (on Si-saturated regions),[14] it is implied that Sn affects C−H bond breaking steps during CH_3 reaction. While speculative, this contention is supported by other studies that have shown that Sn on Pt single crystals diminishes the extent of hydrocarbon decomposition (e.g., of methylacetylene and 1,3-cyclohexadiene) to surface carbon, relative to that on clean Pt.[23−25] Thus, we propose that Sn raises the free energy change for activation of C−H bond cleavage in coadsorbed CH_3 on Si/Cu(100); this is experimentally implied from the increase in T_{max3MS} in the TPD. In this proposition we are assuming that the structural phase (i.e., the ternary c(2 × 2) or the p($\sqrt{2}$ × 3$\sqrt{2}$)R45° phase at higher surface temperatures) is not strongly influencing the desorption mechanism(s). This structural issue will be discussed further in conjunction with deposition on, and desorption from, the Si-unsaturated surface.

4.2 Sn Deposition on Si^{unsat}/Cu(100). The most striking effect due to the presence of Sn, based on our experiments, is the alteration of the product distribution derived from CH_3-TPD for the unsaturated Si/Cu(100) surface (Figure 7). In particular, the addition of Sn on the 0.13 ML Si/Cu(100) surface results in the desorption of $(CH_3)_4$Si (in contrast to $(CH_3)_3$SiH without Sn) with a T_{max4MS} that lies between 350 and 450 K, depending on the Sn coverage. The composition of this peak is mostly (>85%) $(CH_3)_4$Si, with some $(CH_3)_3$SiH also observed. At the highest Sn coverage used (0.7 ML), the 220 and 470 K $(CH_3)_3$-SiH desorption states are eliminated from the TPD profile. Yet, a similar coverage of Sn on the saturated Si^{sat}/Cu(100) surface does not eliminate the 500 K $(CH_3)_3$SiH desorption feature.

The CH_3-TPD data for Si^{unsat}/Cu(100) show a progression in the product desorption kinetics with Sn coverage. Both the 220 and 470 K $(CH_3)_3$SiH desorption features shift to higher temperature as the Sn coverage is raised to a value of 0.37 ML (Figure 7). This gradual behavior suggests a kinetic effect rather than a gross structural change (such as the growth of a new surface domain) in the Sn/Si/Cu(100) structure. As proposed above, the temperature shifts are consistent with a Sn-induced inhibition of C−H bond cleavage, both on the Si^{sat} and the Si^{unsat} regions. This explanation also suggests the reason for the loss in intensity of the ∼220 K feature. If low temperature methyl cracking is completely suppressed, as at 0.7 ML Sn, then methyl still remains on a low Si coverage phase, and a new channel (for tetramethylsilane desorption) can now open up at ∼350 K.

At this point, we must discuss the observed surface structures, their thermal stability, and the implications of their changes on the evolution of desorbing products. First, note that in any TPD scan there is only one tetramethylsilane desorption temperature, T_{max4MS}. Unlike with the Sn-free surface, there is not a second T_{max4MS} associated with desorption from a second (high Si density) phase. In the absence of Sn, the 5 × 13 and disordered phases are believed to exist over the full TPD temperature range. In contrast, with Sn, the observed structures must be changing significantly with ramping temperature, as the Si Auger signal drops rapidly before 420 K (see Figure 4). In LEED, the 0.6 ML Sn/Si^{unsat}/Cu(100) diffraction pattern (see Figure 3c) indicates a p($\sqrt{2}$ × 3$\sqrt{2}$)R45° phase throughout the temperature range. In fact, this periodicity is one that is found over this temperature range for the bimetallic system, Sn/Cu(100), alone. At temperatures above 450 K, this pattern is anticipated, as the Auger indicates an absence of Si. Yet, in the temperature range of 350−420 K, silanes are being produced, and the Auger does show a small Si concentration. Two possibilities exist for the Si placement within the low temperature 0.7 ML Sn/Si^{unsat}/Cu(100) system. Either (i) Si mixes randomly throughout a

poorly ordered p($\sqrt{2} \times 3\sqrt{2}$)R45° phase, or (ii) there can be coexistence of phases, namely the p($\sqrt{2} \times 3\sqrt{2}$)R45° and c(2 × 2) phases. (Note: the diffraction pattern of the former phase contains all the spots of the latter.) In either case, at higher temperatures, (>420 K) there should remain only one phase, the Si-free p($\sqrt{2} \times 3\sqrt{2}$)R45° phase. This is well ordered, as indicated by the strong rise and maximization of the specular helium intensity in Figure 4a. As Si is not present there can be no high temperature $(CH_3)_3SiH$ desorption peak, such as seen from the 0.7 ML Sn/Si^{sat}/Cu(100) surface or from the high silicon density regions in the 0−0.37 ML Sn/Si^{unsat}/Cu(100) surfaces. We propose, therefore, that above 420 K, the 0.7 ML Sn/Si^{unsat}/Cu(100) surface is uniform, albeit somewhat disordered. The Sn serves to suppress methyl cracking below 450 K, and tetramethylsilane is essentially the only desorption product from this surface.

The argument just offered brings forward an important question. Specifically, is the completion of the $(CH_3)_4Si$ desorption feature associated (a) with methyl depletion, or (b) with surface Si depletion from the 0.7 ML Sn/Si^{unsat}/Cu(100) surface? To answer this question we consider the first of two sets of pertinent information. First, we consider the TPD spectra for the 0.37 ML Sn/Si^{unsat}/Cu(100) surface displayed in Figure 7. These data show that the $(CH_3)_4Si$ peak is observed in conjunction with a high T_{max3MS} peak. The implication is that at 500 K some high silicon density phase regions exist [e.g., the 5 × 13, or c(2 × 2)], and that methyl also remains on the surface after completion of the $(CH_3)_4Si$ peak (at ~370 K). At this point, we can refine only our ideas about the completion of the $(CH_3)_4Si$ desorption feature; it is associated either (a) with depletion of *mobile* methyl, or (b) with depletion of Si in what was a low Si concentration phase.

Second, the only additional information we have (relevant to the question above) is that $(CH_3)_4Si$ does not desorb from the 0.37 and 0.7 ML Sn/Si^{sat}/Cu(100) surfaces. Consider, for example, that at 420 K both the 0.7 ML Sn/Si^{unsat}/Cu(100) and 0.7 ML Sn/Si^{sat}/Cu(100) surfaces show p($\sqrt{2} \times 3\sqrt{2}$)R45° LEED patterns, both contain some Si, and both still hold a finite methyl concentration. Yet, the former surface shows $(CH_3)_4Si$ desorption and the latter only $(CH_3)_3SiH$ desorption at higher temperatures. The most obvious difference between the surfaces is in the concentration of surface Si. One might speculate that, at 420 K, the latter surface contains more, if not larger, domains of the c(2 × 2) ternary Sn/Si/Cu structure. How do these domains serve to hinder $(CH_3)_4Si$ desorption? Our somewhat speculative idea is that c(2 × 2) domains act as a retainer of methyl groups. That is, methyl cannot diffuse off these regions to where methyl extractable silicon can be found in the coexisting p($\sqrt{2} \times 3\sqrt{2}$)R45° regions. Support for this idea comes from the interpretation of trimethylsilane desorption from the Sn-free, Si^{unsat}/Cu(100) surface. In that case, it was argued (in the beginning of section 4 above) that methyl must be immobile on the other Si-saturated (5 × 13) regions, otherwise the higher T_{max3MS} peak would not be observed.

We now conclude that, on the 0.37 ML Sn/Si^{unsat}/Cu(100) surfaces, the completion of the $(CH_3)_4Si$ desorption feature is associated with depletion of *mobile* methyl in all regions of low Si concentration. We now also conclude that, on the 0.7 ML Sn/Si^{unsat}/Cu(100) surfaces, where the surface is almost exclusively all p($\sqrt{2} \times 3\sqrt{2}$)R45° in character and all methyl is mobile at 420 K, the completion of the $(CH_3)_4Si$ desorption feature is associated with depletion of all methyl species of this surface.

Note, we have argued that completion of the $(CH_3)_4Si$ desorption feature is *not* due to depletion of Si in a low Si density phase, as any remaining methyl (on this phase) would be prone to decomposition before 500 K. The 500 K desorption feature would then be occurring at lower temperatures, or would not be apparent at all, contrary to the data of the 0.37 ML Sn/Si^{unsat}/Cu(100) surface.

Finally, one other observation needs explanation: $(CH_3)_4Si$ desorption is pushed to higher temperatures as the Sn coverage is raised above 0.37 ML. We speculate that while Sn is believed to increase the net mobility of methyl groups over copper containing surfaces, large Sn coverages may actually hinder this diffusion process. Such coverage dependent effects were implied in an earlier study of Sn diffusing on copper alone.[26]

4.3. TPD from $(CH_3)_4Sn$ Adsorbed on Si/Cu(100). From an XPS study, the amount of Sn on the surface, used for Figure 8, was 0.025 ML. This is comparable only to the lowest Sn coverage data presented in Figure 6. In these $(CH_3)_4Sn$ experiments, $(CH_3)_4Si$ desorption was not observed. This is fully consistent with our observations that Sn coverages in excess of 0.3 ML are required for $(CH_3)_4Si$ production (see Figure 7). Yet, Figure 8 clearly showed that methyl groups were transferred from the tetramethyl tin to the silicon atoms and trimethylsilane evolved. We have argued earlier, in Section 4.2, that methyl was not highly mobile below 500 K on the high Si^{sat}/Cu(100) surface. Yet, $(CH_3)_3SiH$ is seen to desorb from the $(CH_3)_4Sn$/Si^{sat}/Cu(100) surface at temperatures as low as ~250 K. This suggests that when $(CH_3)_4Sn$ was adsorbed on the Si/Cu surface, trimethylated species are easier to form because many of the methyl groups are concentrated by transferal from one Sn center to an individual Si site.

In addition to transference of the methyl groups, the observed production of gaseous $(CH_3)_3SiH$ also requires methyl cracking, with H as an intermediate. On the Si^{sat}/Cu surface, this rate-limiting step, with independently deposited CH_3, is assumed to be operative at temperatures in excess of 500 K. Yet, the T_{max3MS} of Figure 8 appear closer to those observed with independent CH_3 deposition on the Si^{unsat}/Cu surface, namely ~200 K and 450 K, in Figure 7. In the latter case, H formation, methyl cracking, is thought to be promoted by the Cu-rich regions of the nonuniform surface. (The low temperature peak temperature is not exactly reproduced). We have to assume that the presence of a $(CH_3)_4Sn$ species can facilitate some methyl cracking, either at adsorption or as the surface temperature is raised to ~260 K.

The TPD data for $(CH_3)_4Sn$ on the Si^{unsat}/Cu surface also are displayed in Figure 8. The total amount of deposited Sn was also 0.025 ML. Now, with the Si-unsaturated Cu surface, it is less surprising that the observed T_{max3MS} are ~200 K and 450 K, as they are comparable to those observed in Figure 7. Competing effects also may be operating; the Cu-rich regions of the nonuniform surface can promote methyl cracking, and the local Sn atoms may be hindering the same.

5. Summary and General Comments

A study has been presented that has addressed the effects of Sn on the structure of Si/Cu(100) and on the chemistry of CH_3 on Si/Cu(100) with varying amounts of Si. LEED, HAS, ISS, and AES were used to investigate the structural aspects of the Sn/Si/Cu(100) surfaces. In particular, it was shown that the addition of Sn to the Si/Cu(100) surface induced restructuring and the formation of a new ternary SnSiCu c(2 × 2) phase. In general, the addition of Sn to the Si/Cu(100) surface promoted

Si surface loss, either by diffusion into the bulk, or possibly by formation of surface bound microcrystallites on the Si/Cu(100) surface.

With regard to the effect of Sn on the chemistry of CH_3 on Si/Cu(100), there were two significant observations. First, TPD results showed that the desorption temperature of $(CH_3)_3SiH$ increased as the Sn concentration on Si^{sat}/Cu(100) increased. Second, $(CH_3)_4Si$ became the predominate desorbing product at relatively high Sn concentrations on the Si^{unsat}/Cu(100) surface. Both of these experimental observations were explained in terms of Sn suppressing the rate of C−H cracking in adsorbed CH_3 on different areas of the surface. These interpretations, of the experimental results presented in this contribution, are fully consistent with the effects of the Sn promoter in the industrial Direct Synthesis. Specifically, studies of the Direct Synthesis catalyst at real conditions have shown that Sn increases the concentration of methylated (chloro) silane products during industrial reaction conditions and that coking (through CH_3 decomposition) is suppressed. We argue, based on our results, that the experimental observed effects of Sn on the Direct Reaction can be due to suppression of CH_3 decomposition alone on the industrial catalyst, when Sn is present.

Acknowledgment. This research was supported by the National Science Foundation (grant CHE9732798, CHE 0313717) and partial support from Dow Corning Corporation.

References and Notes

(1) Rochow, E. G. *J. Am. Chem. Soc.* **1945**, *67*, 963.
(2) Lewis, L. N. *From sand to silicones, an overview of the chemistry of silicones*; Division of Polymer Chemistry, American Chemical Society: Washington, DC, 1998; Vol. 39.
(3) Yilmaz, S.; Floquet, N.; Falconer, J. L. *J. Catal.* **1996**, *159*, 31.
(4) Larsson, R.; Folkesson, B. *Acta Chem. Scand.* **1996**, *50*, 1060.
(5) Voorhoeve, R. J. H. *Organohalosilanes: Precursors to Silicones*; Elsevier Pub. Co.: Amsterdam, New York, 1967.
(6) Ehrich, H.; Born, D.; Richter, K.; Richter-Mendau, J.; Lieske, H. *Applied Organometallic Chem.* **1997**, *11*, 237.
(7) Floquet, N.; Yilmaz, S.; Falconer, J. L. *J. Catal.* **1994**, *148*, 348.
(8) Friedrich, H. B.; Sevenich, D. M.; Rethwisch, D. G.; Gasper-Galvin, L. D. *Stud. Org. Chem.* **1993**, *49*, 219.
(9) Larsson, R.; Lieske, H. *ACH—Models Chem.* **2000**, *137*, 691.
(10) Gasper-Galvin, L. D.; Sevenich, D. M.; Friedrich, H. B.; Rethwisch, D. G. *J. Catal.* **1991**, *128*, 468.
(11) Gasper-Galvin, L. D.; Rethwisch, D. G.; Sevenich, D. M.; Friedrich, H. B. *Stud. Org. Chem.* **1993**, *49*, 279.
(12) Ward, W. J.; Ritzer, A.; Carroll, K. M.; Flock, J. W. *J. Catal.* **1986**, *100*, 240.
(13) Skinner, H. A. *Advances in Organometallic Chemistry*; Academic Press: New York, 1964; Vol. 2.
(14) Han, J.; Gheyas, S. I.; Wang, Y.; Strongin, D. R.; Graham, A. P.; Hinch, B. J.; Wright, A. P. *J. Phys. Chem. B* **2000**, *104*, 3078.
(15) Han, J.; Gheyas, S. I.; Wang, Y.; Strongin, D. R.; Hinch, B. J.; Wright, A. P. *Langmuir* **2000**, *16*, 6541.
(16) Gheyas, S. I.; Strable, B. L.; Strongin, D. R.; Wright, A. P. *Surf. Sci.* **2001**, *474*, 129.
(17) Potapenko, D. V.; Sysoev, S. E.; Ermakov, A. V.; Hinch, B. J.; Strongin, D. R.; Wright, A. P.; Kuivila, C. *Phys. Rev. B* **2003**, *68*, 075408.
(18) Sysoev, S. E.; Potapenko, D. V.; Ermakov, A. V.; Hinch, B. J.; Strongin, D. R.; Wright, A. P.; Kuivila, C. *J. Phys. Chem. B* **2002**, *106*, 2018.
(19) Goncharova, L. V.; Braun, J.; Ermakov, A. V.; Bishop, G. G.; Smilgies, D. M.; Hinch, B. J. *J. Chem. Phys.* **2001**, *115*, 7713.
(20) Graham, A. P.; Hinch, B. J.; Kochanski, G. P.; McCash, E. M.; Allison, W. *Phys. Rev. B* **1994**, *50*, 15304.
(21) Peng, X. D.; Viswanathan, R.; Smudde, G. H.; Stair, P. C. *Rev. Sci. Instrum.* **1992**, *63*, 3930.
(22) Bishop, G. G.; Graham, A. P.; Mihanic, K.; Wendel, J. K.; Hinch, B. J.; Kochanski, G. P. *Phys. Rev. Lett.* **1997**, *79*, 1409.
(23) Peck, J. W.; Mahon, D. I.; Koel, B. E. *Surf. Sci.* **1998**, *410*, 200.
(24) Peck, J. W.; Koel, B. E. *J. Am. Chem. Soc.* **1996**, *118*, 2708.
(25) Panja, C.; Saliba, N. A.; Koel, B. E. *J. Phys. Chem. B* **2001**, *105*, 3786.
(26) Schmid, A. K.; Bartelt, N. C.; Hwang, R. Q. *Science* **2000**, *290*, 1561.